-RESEARCH PAPER-

International Journal of Mining and Geo-Engineering

IJMGE

IJMGE 57-4 (2023) 413-426

DOI: 10.22059/IJMGE.2023.361937.595082

Hydrocarbon potential evaluation in the Low Resistivity Pays (LRP) of Sarvak formation with combining Nuclear Magnetic Resonance (NMR) and seismic data, one of the hydrocarbon reservoirs in southwest of Iran

Sina Amirnezhad [a], Reza Mohebian [a, *], Abbas Bahrodi [a], Saman Jahanbakhshi [a]

[a] *School of Mining Engineering, College of Engineering, University of Tehran, Tehran, Iran.*

Article History:

Received: 08 July 2023.

Revised: 02 September 2023.

Accepted: 10 September 2023.

ABSTRACT

The objective of petrophysical studies is to assess the quality of hydrocarbon reservoir layers and to zone the reservoir for identifying optimal zones for exploitation and informed development of oil fields. In some regions, there are zones that exhibit lower electrical resistivity values than their actual values. These low-resistivity zones are often identified through petrophysical investigations and conventional well logs, where water saturation levels are estimated higher due to their reduced resistivity. These zones, despite their hydrocarbon potential, are often neglected during production cycles. To overcome this challenge, nuclear magnetic resonance (NMR) logging tools can be employed to provide accurate estimations of free fluid saturation, irreducible fluid saturation, permeability, and effective porosity in such low-resistivity zones, making them more identifiable.

In this article, we utilized conventional well logs and NMR log from the A well in the Sarvak reservoir of one of the oil fields in southwestern Iran. Based on the obtained results, depth interval 9586 to 9783 ft in the Sarvak Formation, along with two intervals (10661-10815 ft) and (10830-11063 ft) in the Int zone, were identified as potential low-resistivity zones in the reservoir. By analyzing the high-resistivity logs, water saturation percentage was calculated for these zones, and the results from NMR logging confirmed their favorable reservoir potential (e.g., free fluid saturation, effective porosity, viscosity, and permeability).

Furthermore, to extend the petrophysical parameters, such as free fluid saturation and porosity, throughout the entire hydrocarbon field, various approaches including single- attribute methods, multi attribute methods, and neural networks were evaluated. The neural network method demonstrated higher accuracy in determining the parameters. Ultimately, the values of porosity and free fluid saturation in the study area were determined with 91% and 95.8% matching accuracy, respectively. The final results were validated using unseen data, and the high precision of the obtained results was confirmed.

Keywords: *Low-resistivity hydrocarbon reservoirs, Nuclear magnetic resonance logging, Petrophysical parameter determination, Borehole distribution.*

1. Introduction

In recent decades, there has been significant attention in the field of geology and hydrocarbon exploration towards the exploration and characterization of low resistivity pay zones in petroleum reservoirs [1-2]. Electrical resistivity imaging tools can provide relatively accurate interpretations of the presence and quantity of hydrocarbons, as well as the contact boundary between water, oil, and gas [25]. The principles of this method are based on the electrical current flow within the formation and the registration of its return response. As long as the formation is conductive, the device records low resistance values, while if the formation contains hydrocarbons, it registers high resistivity values. Sometimes, due to certain reasons, the resistivity against the reservoir layers decreases, leading to these reservoir layers being identified as the low resistivity reservoir zones. Resistivity logs can indicate very low resistivity values against low-resistivity zones, and conventional saturation calculation methods often utilize resistivity log results, resulting in errors and unrealistic values for low-resistivity layers. This can lead to the exclusion of these layers during field development stages, reducing production potential. Identifying, characterizing, and evaluating low-resistivity reservoirs are highly challenging and significant tasks in oil and gas field development [3]. Additionally, it can be stated that these low-resistivity zones are formed in deepwater depositional environments, deltaic deposits, turbidites, and alluvial channels [14]. The causes of resistivity reduction in hydrocarbon reservoirs can be classified into internal and external factors. Internal causes mainly include highly saline formation water, immobile irreducible water saturation resulting from fine pore throats development, excessively conductive clays, and thin sand and shale layers. External factors, on the other hand, include the invasion of saltwater and limited resolution power of resistivity logging tools, especially in the presence of a borehole's invasion, which causes thin shale layers to be poorly identified due to their unresolvable nature by the resistivity logging tools. Also, the low resistivity of shale layers is considered, leading to the resistivity logging tool treating shale and sand layers as a single layer and averaging their properties, causing it to show

* Corresponding author. *E-mail address:* mohebian@ut.ac.ir (R. Mohebian).

shale layers as having lower resistivity values than their actual values [11].

The creation of low-resistivity reservoirs can be primarily categorized into two groups: the first mechanism includes reservoirs where actual water saturation is high, but water-free hydrocarbons are being produced. This mechanism is usually attributed to small-scale porosity. The second mechanism includes reservoirs where calculated water saturation exceeds the actual water saturation. The high amounts of water saturation are caused by the presence of conductive minerals such as clays and pyrite in the clean reservoir rocks [11-13].

In 2022, Kelishami and colleagues analyzed microscale porosity and natural fractures in carbonate reservoirs in southern Iran. They determined that porosity is a vital property of a reservoir rock; however, in the production context, the connectivity of pores must be considered. Different connected pores play a crucial role in the reservoir quality, and the impacts of various clay minerals should also be taken into account. Clay minerals such as illite and kaolinite may directly influence the reservoir quality by obstructing pores and filling free spaces. Through the integration of core data, well logs, seismic data, and microscopic thin-section analysis, a comprehensive overview of the reservoir properties in a hydrocarbon field can be obtained [12].

To address this challenge, Nuclear Magnetic Resonance (NMR) logging data were employed in this study to determine fluid saturation in potential low resistivity reservoirs. Furthermore, the mechanisms and factors leading to the formation of these zones in the Sarvak reservoir were investigated. Additionally, the correlation between seismic data and influential parameters in identifying low resistivity zones, aiming to accurately distribute potential low-resistivity zones throughout the entire Sarvak reservoir field, has been utilized in this study. The criterion focused on in this research is based on the percentage of free fluid saturation, effective porosity, and calculated irreducible water saturation from NMR logs. The aim of this study is to identify low-resistivity reservoir layers and the reasons for this phenomenon in hydrocarbon reservoir layers. Furthermore, it aims to detect such reservoir layers using NMR logging data, determine their distribution using three-dimensional seismic data throughout the reservoir, and ultimately achieve accurate calculations of free fluid saturation in reservoir layers. Additionally, obtaining precise petrophysical parameters such as porosity, necessary for constructing a suitable reservoir model, is another part of the objectives of this research.

2. Geology

The studied field is located in the southwest of Iran, 80 km west of Ahvaz, close to the Sosangerd city and to the Iran-Iraq border [23]. The oil field under study is in Abadan Plain, situated parallel to the Iran-Iraq border and in the vicinity of Majnoon and Nahr Umar structures in Iraq [23].

Abadan Plain is an important oil region in the southwest of the Dezful basin in Iran. This region is also positioned in the extreme southwest of Zagros. Structurally, Abadan Plain is part of the Mesopotamian sedimentary basin in Iran [7]. It marks the northern end of the Arabian platform, displaying a north-south structural trend in contrast to the northwest-southeast trend of Zagros. I apologize for the oversight. Here's a version that adheres closely to the original text.

The studied field is located in the southwest of Iran, 80 km west of Ahvaz, near the city of Sosangerd, and close to the Iran-Iraq border [23]. The oil field under study is in Abadan Plain, situated parallel to the Iran-Iraq border and in the vicinity of Majnoon and Nahr Umar structures in Iraq [23].

Abadan Plain is an important oil region in the southwest of the Dezful basin in Iran. This region is also positioned in the extreme southwest of Zagros. Structurally, Abadan Plain is part of the Mesopotamian sedimentary basin in Iran [7]. It marks the northern end of the Arabian platform, displaying a north-south structural trend in contrast to the northwest-southeast trend of Zagros. Furthermore, it is a low-flooding plain covered by young alluvial sediments affected by the Zagros orogeny [23]. Fig 1 illustrates the location of different structural zones in the south and southwest of Iran, along with the geographical map of the studied area.

The studied field presents a symmetrically folded structure with gentle slopes. The surface of this geophysical structure is not outcropped and is covered by present-day alluvial deposits [7].

The main reservoir in this field is the Sarvak formation, composed of carbonate rocks. The Sarvak formation reservoir contains heavy oil, with its source rock being the Shili-Marne Pabdeh and Gurpi formations [7].Fig 1 illustrates the location of different structural zones in the south and southwest of Iran, along with the geographical map of the studied area.

The studied field presents a symmetrically folded structure with gentle slopes. The surface of this geophysical structure is not outcropped and is covered by present-day alluvial deposits [7].

The main reservoir in this field is the Sarvak formation, composed of carbonate rocks. The Sarvak formation reservoir contains heavy oil, with its source rock being the Shili-Marne Pabdeh and Gurpi formations [7].

The Sarvak Formation is a geological formation within the Bangistan Group in Zagros, dating back to the Middle Cretaceous age. Regarded as one of the significant hydrocarbon reservoirs in the Zagros basin, this formation plays a crucial role in the region's geology [24].

In this oil field, the Sarvak Formation, with a thickness exceeding 600 meters, is situated between the Dariyan Formation at the bottom and the Ilam Formation at the top. This formation consists of a thick sequence of limestone and interlayers of marly limestone, and therefore, no significant lithological changes are observed in it [16]. The uplift and erosion of the upper Sarvak carbonate platform during the Cenomanian period caused it to emerge from the water, resulting in a lack of sedimentation in parts of the Zagros sedimentary basin. Consequently, an expansion of channel deposits was reported in the Sarvak Formation of this field during the Cenomanian [16].

In addition to the Sarvak Formation, the Ilam and Fahliyan formations are also considered as well-known reservoir sections in this field. The primary Sarvak reservoir, known for its burial depth ranging from about 2600 to 3000 meters and exhibiting bioclastic limestone lithology, constitutes 92% of the total hydrocarbon reserves [16-9]. The Sarvak reservoir is divided into 12 sub-layers, with sub-layer S-3, due to its high porosity and low water saturation, having the highest production rate among other parts of the Sarvak Formation [9].

After the Sarvak formation reservoir, the Kazhdumi sandstone reservoir layer can be referred to, constituted by alternating layers of shale and sandstone. In this field, the sandstone layers contain light oil, and the broad distribution of hydrocarbons in the studied area suggests a robust source rock in the Garu Formation [7-10]. The primary cap rock for the Sarvak and Ilam reservoir layers is represented by the Lafan and Gurpi formations, along with intermediate shale layers within these reservoirs [27].

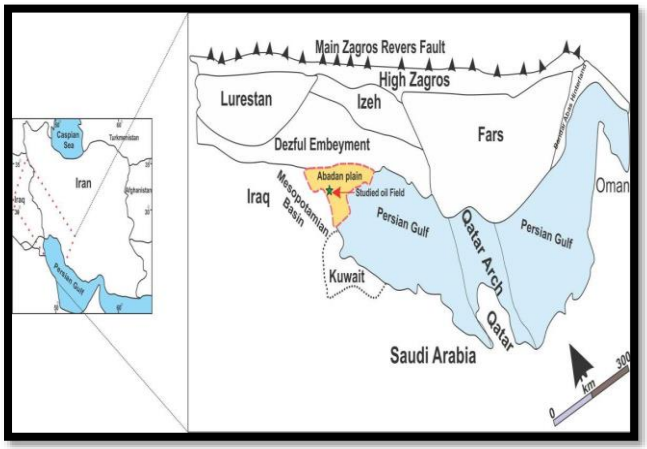

Fig. 1. The location of different structural zones in the south and southwest of Iran is shown [24].

The Kazhdumi formation in this field is categorized into three parts—lower, middle, and upper—based on changes in the gamma-ray diagram and petrographic studies. The lower part comprises sandstone, the middle part consists of limestone, and the upper part is composed of clay limestone. The lower border of the Kazhdumi formation with the Dariyan formation is erosional due to the presence of hematite nodules and oxidized sediments, while the upper border with the Sarvak formation is gradual. Deposited during the Cretaceous Albian stage, the Kazhdumi formation is in contact with Sarvak. The stratigraphic column of the studied field in the Zagros Basin is depicted in Fig 2 [27].

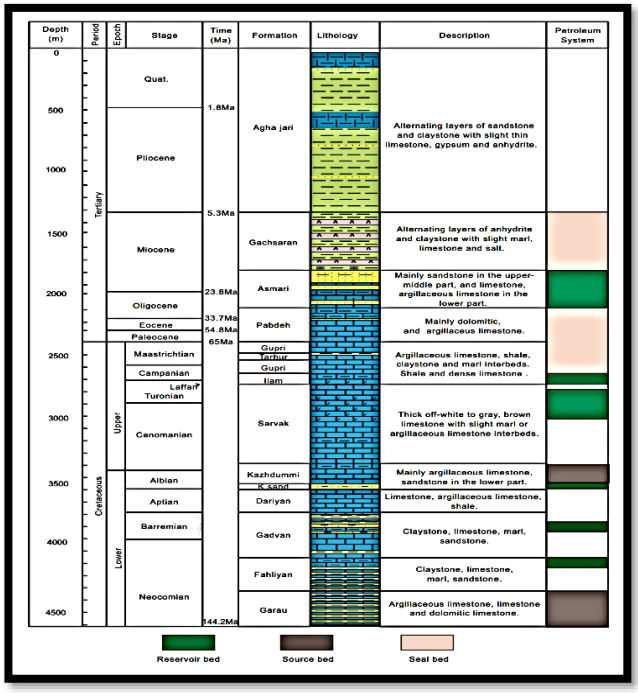

Fig. 2. Stratigraphic column of the Zagros Basin [27].

3. Methodology

The data used in this research include full-suite well log data (such as resistivity, neutron, density, sonic, and gamma logs) as well as advanced nuclear magnetic resonance (NMR) logging data acquisition from a well in the studied field.

Initially, the available well data were imported into the Geolog software. Before entering the petrophysical computation cycle, certain steps such as data quality control, environmental corrections, and depth matching of the data needed to be executed. Following quality control and data editing, preliminary calculations were conducted on the data. Various parameters, including density, salinity, drilling mud resistivity, reservoir temperature and pressure, well diameter, mud cake thickness, and wall rugosity or invasion of the wellbore, were taken into account as influential factors on different log responses. These factors were considered for corrections and evaluations. Subsequently, environmental corrections were applied, and all factors affecting the tool response in the vicinity of the sonde were examined.

After extracting the NMR results, the distribution of these data throughout the entire field will be determined using available 3D seismic data. In this regard, the acoustic impedance resulting from the inversion of seismic data, along with other seismic indicators using multi-parameter methods, probabilistic neural networks, and multi-layer feed-forward neural networks, will be employed to estimate and evaluate key parameters such as free fluid saturation, effective porosity, and permeability in the reservoir layer. Finally, for validation purposes, blind test and trained data points are used to verify the results.

In the presence of hydrocarbon-bearing low-resistivity zones, using conventional petrophysical analyses and common log plots, the water saturation levels have been calculated to be high due to their reduced resistivity. Based on this, the NMR log can differentiate between free fluids (fluids producible in large voids) and bound fluids (fluids immobile in small voids) based on the decay of hydrogen signals in the porous space and determine the amount of producible fluid in each zone [17]. It is possible that in a zone, the calculated water saturation using the probabilistic method may be high, but after NMR evaluations, it is determined that this zone has a significant amount of non-producible water associated with the bound fluid.

3.1. Nuclear Magnetic Resonance (NMR) Logging

NMR logging relies on a simple principle involving the manipulation of molecular behavior using a magnetic field. Some atomic nuclei, such as hydrogen, carbon, nitrogen, and phosphorus, possess magnetic properties. The proton in a hydrogen nucleus is the simplest case of nucleus magnetization.

Initially, the alignment of protons within the formation fluid is random and isotropic. However, when placed in a static magnetic field (Bo), the protons align themselves in the direction of the field. This magnetic field polarizes the proton spins, aligning them. Subsequently, an oscillating magnetic field (low-energy radiofrequency) is applied to deviate these protons from their new equilibrium positions. When the oscillating field is turned off, the protons tend to return to their permanent magnetic field state (equilibrium state). During this relaxation, they emit signals recorded by the logging tool. These signals are recorded in the form of a decaying exponential curve, and by analyzing these curves, the petrophysical properties of the reservoir are evaluated [15].

Successive CPMG (Carr-Purcell-Meiboom-Gill) pulses generate a series of spin echoes, and the NMR tool records these echoes, constituting the raw data. The tool measures the NMR echo amplitude as a function of time to produce the series of spin echoes. Due to the tool's constant speed over a short period, it can only investigate and assess a small volume of the formation, referred to as the sensitive volume. This sequence of echoes is linked to fluid-filled porosity and parameters such as TE (time between echoes in a pulse sequence) and TW (time between the last measurement of an echo and the start of the next echo). It is also associated with several petrophysical properties such as T1 (longitudinal relaxation time of flipped protons relative to the magnetic axis), T2 (transverse relaxation time of flipped protons relative to the magnetic axis), HI (hydrogen atom density in the fluid), and D (indicating how far molecules within the fluid can diffuse randomly) [4].

3.2. Evaluation of Porosity Parameter

Accurate calculation of rock porosity plays a crucial role in reducing uncertainty in simulation and reservoir modeling processes. The T2 decay curve, representing the decay of received signals from hydrogen nuclei under the influence of the applied magnetic field, corresponds to empty spaces and is proportional to the size of the pores. Essentially, smaller pores exhibit shorter T2 values, while larger pores display longer T2 values. The overall T2 distribution curve reflects the summation of these individual curves, thereby representing the pore size distribution. Calculating the area under the T2 distribution curve enables the determination of the total effective porosity of the rock. The initial amplitude of the relaxation curve obtained from NMR measurements is contingent upon the number of polarized hydrogen nuclei within the fluid present in the pore. Consequently, the amplitude can be calibrated to derive porosity. This porosity is independent of lithology and can be validated by comparing it with laboratory NMR measurements on core samples or conventional laboratory measurements. In a porous medium, the T2 relaxation time is directly proportional to the size of the empty spaces [6-20]. The observed T2 decay corresponds to the sum of signals from multiple empty spaces, each with its own relaxation time. The graphically presented T2 distribution (third column in Fig 5) indicates

the volume of fluid associated with each T2 value, corresponding to the volume linked with each empty space [4].

Based on the NMR data acquired from the well and subsequent processing steps, seven constant T2 values are considered for classification purposes: 1, 3, 8, 16, 32, 100, and 512 milliseconds. The T2 distribution is divided into eight equal parts, with each part referred to as a bin. It can be understood that each bin represents a group of pores with a specific size. This process of partitioning the porosity distribution is known as binning [4]. Porosity binning is utilized to determine the size of the pores within the formation. The resulting pore distribution in the Sarvak reservoir of Well A is depicted in Fig 3.

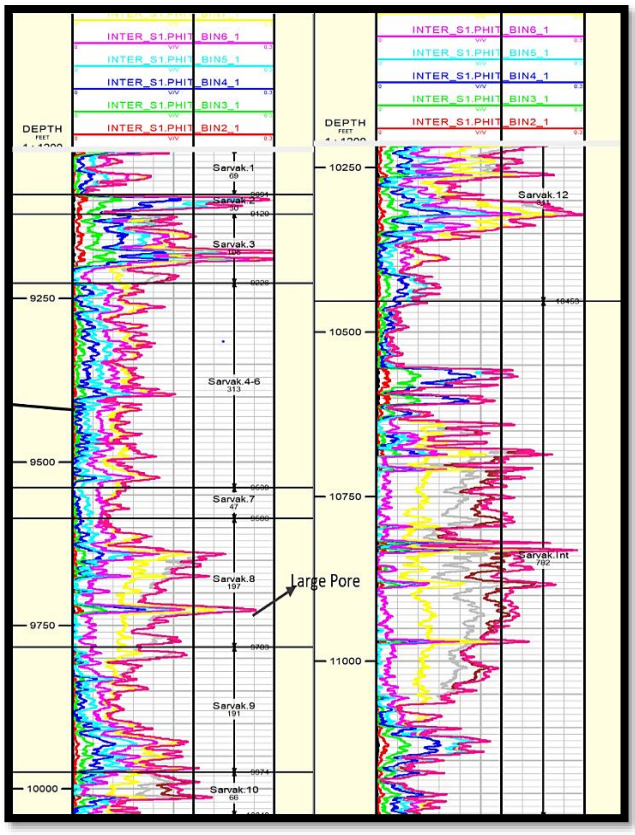

Fig. 3. The Pore size distribution is shown for ten different bins with distinct colors. In this Fig, from right to left, the extremely fine pores are initially represented, followed by larger pores indicated by different colors. Some of them are highlighted with arrows as samples in the Fig.

3.3. Determining the volume of free fluid and irreducible fluid

Interconnected water, bound water, and free water occupy pores of different sizes and locations. Hydrocarbon fluids, in contrast to saline water, typically occupy larger pores and exhibit different viscosity and diffusivity characteristics. NMR logging leverages these distinctions to identify fluids within pore spaces. Generally, bound water and bound mud fluids have very short T1 and T2 relaxation times, and their diffusion is slow due to molecular confinement in small pores [6]. Table 1 provides the T2 values for various reservoir fluids.

Table 1. NMR Characteristics for Reservoir Fluids [6]

Fluid	T1 (ms)	T2 (ms)	T1/T2	Viscosity (Cp)
Water	500-1	500-1	2	2/0 - 8/0
Crude Oil	4000-3000	1000-300	4	2/1 - 1000
Gas	5000-4000	60-30	80	011/0 - 014/0

3.4. Determining the Free Fluid and Irreducible Fluid Volumes

The obtained porosity from NMR logging, denoted as "ϕr", along with other porosity-related curves, can be used to calculate Swirr. The term "ϕe-ϕr" represents the difference between effective porosity and fluid saturation, indicating the occupied porosity by immobile fluids. This can be expressed by Equation 1:

$$\phi bound = (\phi e - \phi f) \quad (1)$$

Therefore, to normalize this value by the effective porosity, Swirr can be obtained as shown in Equation 2:

$$\text{Swirr} = \frac{(\phi e - \phi f)}{\phi e} = \frac{\phi Bound}{\phi e} \quad (2)$$

Fluids exist in pores of varying sizes, categorized as: a) Water trapped in clays, b) Water in pores where capillary forces have a significant impact on fluid movement, c) Fluids that can easily move in large spaces.

To calculate the percentage of free fluid saturation, it is sufficient to subtract the total porosity obtained from the NMR curve from the water saturation curve and obtain the percentage of free fluid saturation. This relationship can be expressed by Equation 3:

$$\text{Free Fluid Saturation} = \{PHIT(NMR) - BFV(NMR)\} \quad (3)$$

Different types of fluids exhibit varying diffusion coefficients. Generally, free water demonstrates average T1 and T2 values. Hydrocarbons, including natural gas, light oil, medium, and heavy oil, also display distinct NMR characteristics. Natural gas exhibits long T1 times, short T2 times, and a unique relaxation response. The NMR characteristics of oil vary widely and strongly depend on oil viscosity. Lighter oils are more mobile, featuring longer T1 and T2 times and often showing a distinctive relaxation response. As the oil becomes heavier and the hydrocarbon composition becomes more complex, the diffusion, T1, and T2 times decrease.

In general, fluids confined in small spaces exhibit short T1 and T2 times and low diffusion coefficients due to molecular movement restrictions in such spaces. Therefore, NMR is commonly employed to determine the volumetric fraction of fine-grained layers, such as shale (resulting in a decrease in electrical resistivity in layered formations), by analyzing the pore size distribution obtained from the T2 distribution curve. This volumetric fraction includes layers with the highest water saturation trapped in clays and affected by capillary forces. Reservoirs with low resistivity can lead to incorrect interpretation of logging data, potentially overestimating water saturation. The NMR method addresses this issue by providing information not only about porosity and fluid type but also about water trapped in clays, bound water, and mobile water [15].

Based on Fig 4, the T2 distribution curve can be utilized to delineate the distribution of producible and non-producible fluids based on a threshold in the Sarvak Formation. As evident from the figure, there are significant producible fluids present in this formation.

In fact, T2 for crude oil is not merely a numerical value; it is a distribution that depends on the oil viscosity. As viscosity increases, hydrogen atoms move less and reach relaxation more quickly. Therefore, an increase in viscosity results in a reduction in the geometric mean of T2, and oils with higher viscosity also exhibit different T2 distributions [6].

3.5. Determining the T2 Threshold

Considering that T2 values are related to the size of the porous space, it is possible to separate fluids located in small pores from those in larger pores by setting a specific T2 value, referred to as the T2 threshold. Therefore, the T2 threshold is an input parameter used to classify porosity into two categories: free fluid and bound fluid. If a pore volume is above the threshold, it has the ability to produce fluids. In the interpretation performed, the T2 threshold value is observed in the red curve in Fig 5, and for this case, it is considered to be 100 milliseconds.

Determining the threshold value is mineralogy-dependent and is empirically determined for sandstones and carbonates. Laboratory data

suggest values of 33 milliseconds for sandstones and 100 milliseconds for carbonates. The longer value in carbonates can be attributed to relaxation time in carbonates. The T2 relaxation curve typically ranges between 0.3 to 3000 milliseconds. It should be noted that the area under the curve is proportional to the total porosity, ranging from 0.3 to 3 milliseconds for clay-bound water, from 3 to 33 milliseconds for clay porosity, and from 33 to 3000 milliseconds for producible fluid porosity. By combining the pore volumes in the lower section below the threshold, the volume of immobile water can be obtained. This quantity is an important petrophysical parameter that helps determine the maximum fillable pore volume by hydrocarbons. Therefore, a value called T2 Cutoff is considered, below which fluids are located in small pores, and above which fluids are located in larger pores, as shown in Fig 5. The separation of free fluid (FFI) and bound volume irreducible (BVI) is achieved by the distribution of T2 and T2 Cutoff. Inversion is used to determine the subsurface distribution of T2. The precise interpretation of the subsurface T2 distribution provides information about the pore size, fluid type, and hydrocarbon volume, which is continuously interpreted as a function [5]. In this study, the T2 threshold value is estimated to be 100 milliseconds based on the provided information.

According to Fig 5, the T2 distribution function illustrates the Sarvak reservoir intervals where various values of T2 relaxation time, fluid production threshold, and the distribution plot of T2 abundance coexist. Based on these values, it can be inferred that there are productive zones in the Sarvak reservoir, considering the threshold value set for producible fluids (red curve).

3.6. Calculation of Reservoir Rock Permeability

In the NMR method, the permeability of the rock is calculated based on the empirical relationships between the calculated porosity and the average relaxation time, T2 [4].

Permeability using the SDR model: One of the most significant formulas developed by SDR Company is the equation relating permeability to T2 using measurements obtained from NMR permeability and hundreds of core samples in the laboratory. This equation is expressed as follows (Equation 4):

$$KNMR = C\left(\phi^{4}\right) * (T2\ lm^{2}) \quad (4)$$

In this formula, C is a coefficient proportional to the lithology type of the rock (4 for sandstones and 0.1 for limestone), ϕ is the measured porosity using NMR, and (T2) LM is the logarithmic mean of the T2 relaxation time distribution [4].

Permeability using the Timur-Coates model: Another method for calculating rock permeability is using the Timur-Coates formula (Equation 5), which is proportional to the ratio of producible water saturation ϕFF to the water trapped in the micropores ϕBF due to high capillary pressure.

$$KNMR = 1000 * \left(\frac{\varphi FF}{\varphi BF}\right)^{2} * \varphi^{4} \quad (5)$$

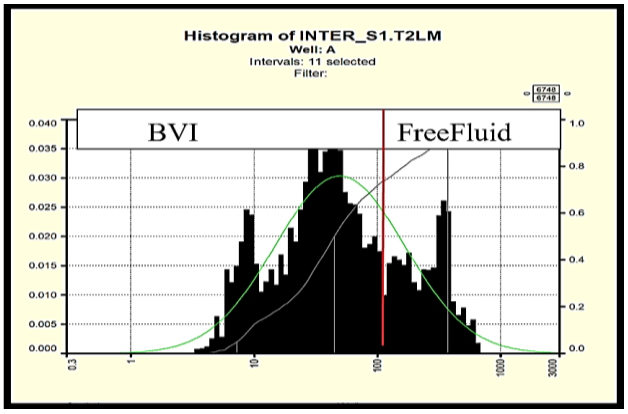

Fig. 4. Separation of T2 distribution for free fluid and immovable fluids.

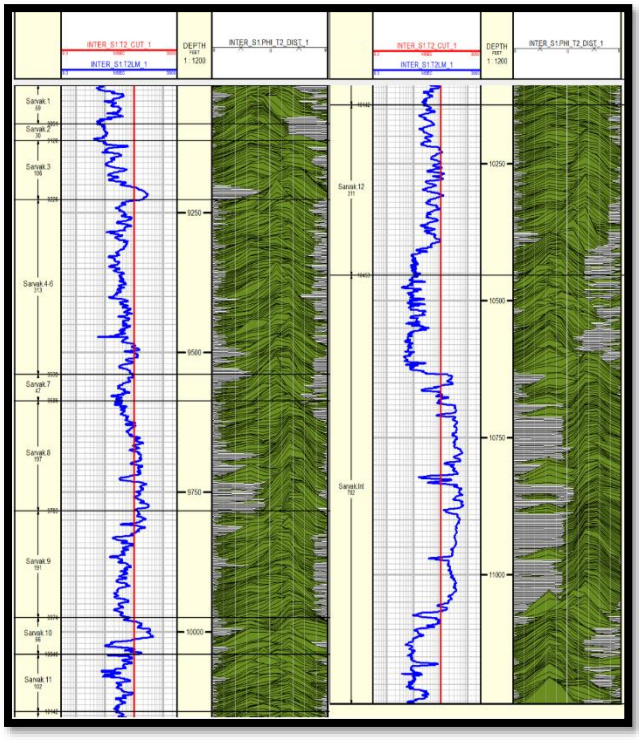

Fig. 5. The T2 distribution function in the Sarvak reservoir of Well A is shown in the left-hand plot, covering the intervals from 1 to 10, while the right-hand plot represents the intervals from 11 to Int.

According to the mentioned formulas, both permeability models incorporate an important and indicative parameter that forms the basis of their formulas, representing the description of the surface-to-volume ratio changes in the porosity. In the Timur-Coates model, the FFI/BVI ratio is used, while in the SDR model, the geometric mean logarithmic $T2$ is used to demonstrate the effect of surface-to-volume ratio changes in permeability calculation. In fact, based on the NMR data, it is possible to distinguish permeable layers from impermeable ones. In regions where the $T2$ distribution tends to increase, the values of KTM and $KSDR$ also increase, indicating a permeable layer. Fig 6 shows the permeability curve of the Sarvak reservoir calculated based on empirical NMR formulas [4].

3.7. Determination of Viscosity from the T2LM Parameter

Considering the specific definition and nature of viscosity, which represents the resistance of a fluid to flow, this parameter is highly useful in evaluating and identifying the type of reservoir fluid, obtained from NMR chart results. $T2LM$ is, in fact, the geometric mean of the $T2$ distribution and is calculated by taking the logarithmic average of relaxation times in each distribution. Logarithmic $T2$ distribution is used to assess the viscosity parameter. Additionally, the viscosity value is evaluated based on equation 6.

$$\text{Viscosity} = \left(\frac{1.2}{T2\ lm}\right)^{\frac{1}{0.9}} \quad (6)$$

Based on the classification of different types of oil in reservoirs, light oils have low viscosity, high API gravity, and low density compared to heavy oils. Furthermore, the viscosity values of reservoir fluids are provided in Table 1. It is worth nothing that in the case of membrane fluids in the reservoir with different temperatures, they have an impact on the viscosity parameter. Therefore, it is recommended to use core data for accurate identification of the type of free fluid. In Fig 7, the distribution of viscosity chart in the Sarvak reservoir is deoicted. With an increase in viscosity, the mobility of hydrogen protons decreases, resulting in a shorter relaxation time. Hence, an increase in the average geometric $T2$ shortens the relaxation time. Oils with higher adhesive

properties usually have broader T2 distributions, which is attributed to the different mobility of proton compounds in various oil compositions. It should also be noted that when the temperature of the fluid increases, the intermolecular forces of the fluid decrease, leading to a decrease in viscosity.

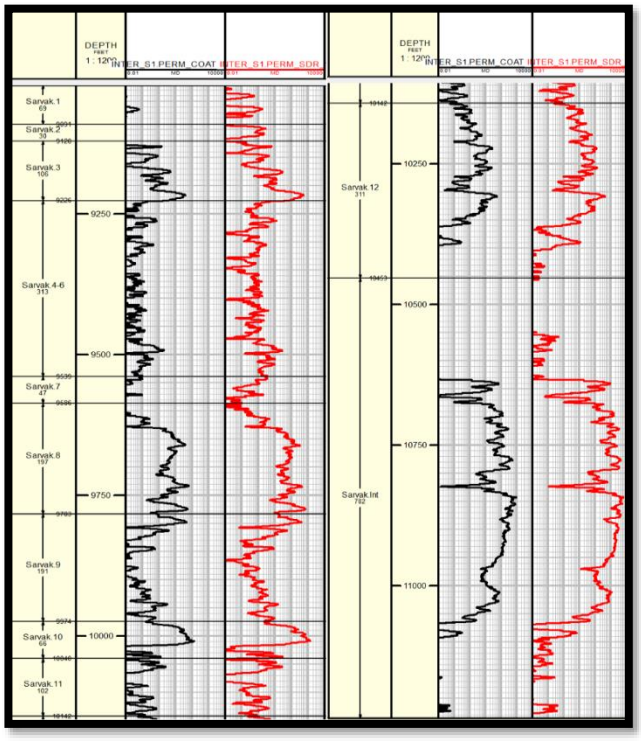

Fig. 6. Permeability Chart Calculated from SDR and Timur Formulas in the Sarvak Reservoir, Well A. The chart on the left represents the permeability range from 1 to 10, and the chart on the right represents the permeability range from 11 to Int.

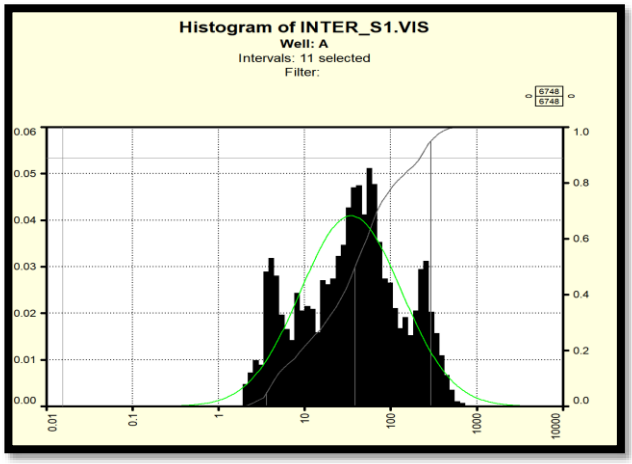

Fig. 7. Distribution of Viscosity Chart in the Sarvak Reservoir. With an increase in viscosity, the mobility of hydrogen protons decreases, resulting in a shorter relaxation time.

3.8. Resistivity Logs in Well Logging

Resistivity logs calculate one of the petrophysical parameters (i.e. the estimation of water saturation) using existing relationships. With resistivity log data and water saturation calculation formulas, this parameter is evaluated. Measuring formation resistivity is crucial for assessing hydrocarbon saturation. Resistivity logs can accurately interpret the presence and quantity of hydrocarbons, as well as the contact boundary between water, oil, and gas. The method's principles are based on the electrical conductivity within the formation and the recording of the corresponding response. If the formation is conductive, the logging tool will record a low-resistivity value. In contrast, if the formation contains hydrocarbons, a high-resistivity value will be recorded. Formation resistivity is influenced by parameters such as formation water resistivity, the amount of water present in the rock (dependent on porosity), and the geometry and structure of the pore spaces.

The calculation of water saturation using electrical resistivity techniques has been employed since the 1940s. Archie formulated his conclusions based on clean sand samples collected from the Gulf of Mexico. Determining water saturation in hydrocarbon reservoirs is carried out using well logs and applying water saturation formulas. Equation 7 has been introduced by Archie to calculate water saturation in clean sand formations, considering changes in actual formation resistivity (Rt) and formation water resistivity (Rw) with the known porosity (φ) [18].

$$Sw = \sqrt[n]{f} * \frac{Rw}{Rt} \quad (7)$$

Since Archie's equation is utilized for water saturation calculations, it presents several limitations in shale formations. The equation fails to consider the impacts of shale components, shale content, and cation exchange capacity. This oversight often results in an overestimation of water saturation, leading to the formation of reservoirs with low resistivity. In such instances, there is a necessity to formulate water saturation models tailored to various shale formations. The percentage of porosity can be accurately determined using available porosity logs such as sonic, density, and neutron logs, and it can then be substituted into the Archie equation. However, when employing resistivity logs, the calculated value is consistently associated with a significant margin of error due to the presence of shales and clay impurities in the reservoir rock, along with the type of fluid present in the formations. Research indicates that even a small percentage of clay minerals like kaolinite, illite, and montmorillonite in the reservoir rock leads to higher water saturation values when using the well-known Archie formula. This increase is attributed to the decrease in formation resistivity [18].

3.9. Inversion

Seismic inversion is a unique method used to extract reservoir properties from seismic data [19]. The careful selection of seismic inversion methods is crucial for determining reservoir quality parameters. Through seismic inversion, the acoustic impedance can be determined more accurately compared to other methods, facilitating the precise interpretation of reservoir horizons. Various methods for the seismic inversion process, such as constrained sparse spike inversion, model-based inversion, sparse-spike inversion, and color inversion, have been defined in Hampson-Russell software. In this study, the model-based and sparse-spike inversion methods are compared, and the best-performing method is selected [19].

Model-based inversion

In the model-based algorithm, a general linear mathematical relationship is applied between synthetic seismic response and observed seismic response. The model is adjusted based on the difference obtained from comparing the two responses to achieve a close match (within an acceptable error range). A control parameter is used to determine the termination or non-termination time of the algorithm. This is done to prevent small noise and modeling errors from entering the data and to avoid erroneous inputs to the algorithm. In the model-based method, the acoustic impedance behaves like blocks, and the problem of non-units in the inversion results is addressed by limiting the number of layers relative to the number of seismic samples. This method is more sensitive to the initial model and wavelets compared to other methods. In this method, low-frequency information can be recovered, unlike other methods [21-22].

The model-based inversion algorithm is employed on the seismic volume with the parameters outlined in Table 2, and the percentage of fit and error at well locations A and B are acquired as presented in Table

3. Figure 8 illustrates the outcomes of applying this method at well location A.

Table 2. Optimal Variable Parameters in the Model-Based Algorithm.

Average Block Size	4 milliseconds
Iteration Parameter	20
Hard Constraint	5
prewhitening	1

Table 3. Correlation Coefficient and Error in the Results of Model-Based Inversion at Well Locations.

Model Base	Well A	Well B
Correlation Coefficient	99%	99%
Error Rate	0.039	0.048

In this method, the more iterations are performed, the more accurate the constructed model will be, but the computation time will increase. Similarly, a smaller block size will result in a more accurate model, but it introduces higher error due to noise. It is better to have a slightly higher sampling rate for seismic data to mitigate this issue. Considering these factors, the combination of the initial low-frequency impedance model and the limited-bandwidth impedance model obtained from seismic mapping is addressed. Various algorithms exist for integrating these data [22]. Fig 8 illustrates the wide-bandwidth impedance model for a seismic section at Well A. As observed, reservoir interpretation under these conditions is much easier compared to interpretation based on the initial seismic section, and changes in lithology in both horizontal and vertical directions are easily discernible. The seismic data inversion was performed in the interval between the base and top of the Sarvak Formation, as shown. The color range indicates the impedance range, with green representing the lowest impedance and purple representing the highest impedance. They are clearly delineated from each other.

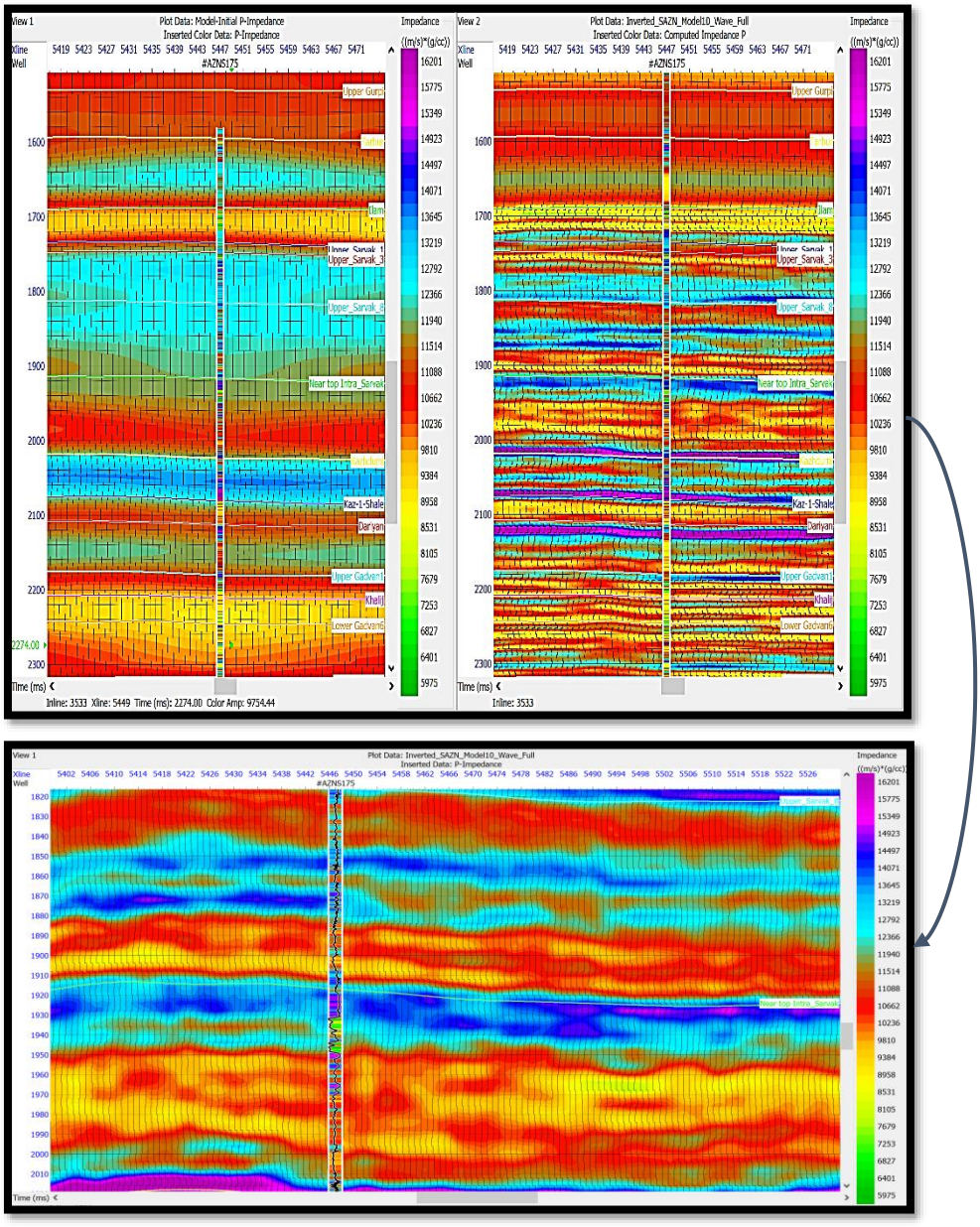

Fig. 8. On the right side, the final wide-bandwidth impedance.

According to Fig 8b), it is apparent that the acoustic impedance exhibits a good match with the final model at Well A. Furthermore, in the intervals of (1850-1820 ms), (1910-1880 ms), and (2000-1950 ms), the acoustic impedance reaches its minimum value in the wellbore section. This suggests the presence of factors such as porous media and reservoir fluids in these intervals, influencing the acoustic impedance curve. It is noteworthy that the acoustic impedance derived from the sonic and density logs of Well A also validates these findings.

4. Discussion

4.1. Determining the type of porosity in the reservoir

To identify the type of porosity in the studied reservoir, the cross-plot of porosity versus permeability can be employed. By interpreting the cross-plot and comparing it with Fig 9, it can be inferred that the porosity in the studied reservoir is primarily granular, encompassing microscale porosity and fractures. As mentioned previously, the existence of fractures and microscale porosity plays a role in the creation of low-resistivity zones within the reservoir [5].

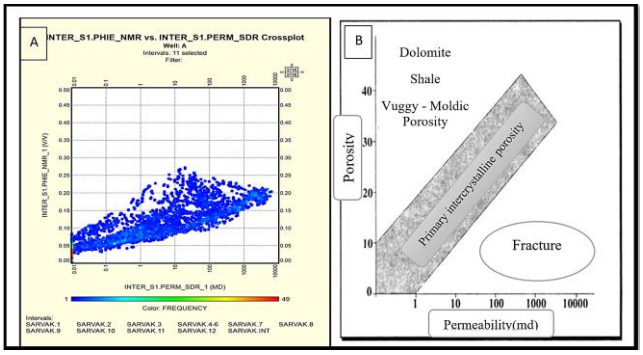

Fig.9. a) NMR core porosity cross-plot against permeability for the Sarvak reservoir. Fig 9b) A summary of the relationship between porosity and permeability and the determination of porosity types [5].

4.2. Comparison of water saturation obtained from resistivity logs and NMR logs

In the magnetization enhancement log, the volume of bound fluid has two definitions: a) the water that remains in the pore space and is not produced during reservoir production, and b) the water that is immobile and confined within its own space when hydrocarbons enter the reservoir [8]. In Fig 10, the calculated fluid saturation from NMR measurements is plotted against the water saturation obtained from resistivity logs. Based on this plot, it can be concluded that in some zones, due to the increased shale volume, the water saturation calculated from the resistivity logs is significantly overestimated. In contrast, the fluid saturation obtained from NMR provides a more detailed evaluation of the producible fluid and immovable water in these intervals, including connate water, clay-bound water, and restricted water. By comparing the water saturation from the resistivity logs with the NMR results, it is possible to determine the interference level in the production process. This enables petrophysicists to quantify the producible and non-producible fluid present in the reservoir zones.

In Fig 10, as indicated in the legend, the black curve represents microporous water, the red curve represents free fluid, the green curve represents restricted clay-bound water, the dark blue curve represents irreducible water, and the light blue curve represents low saturations of water. These water saturations are calculated from the resistivity logs. As observed, this plot yields very high saturation values. Additionally, the range of all values is within 0-0.5%, limited by the very low saturations obtained from the NMR logs, whereas the resistivity logs indicate higher saturation values, exceeding the predefined range.

The probabilistic interpretation of water saturation is calculated using methods such as Archie and Indonesian equations. Considering the aforementioned points, the shortest times are associated with the presence of clay-bound and microporous water, defined as bound fluid volumes. It should be noted that the volume of microporous water can be calculated by summing the microporous water and the clay-bound water according to Equation 8.

$$BFV=BVI+CBW \quad (8)$$

Where,
BVI: Bulk Volume irreducible
CBW: Clay Bound Water
BFV: Boundry Fluid Volume

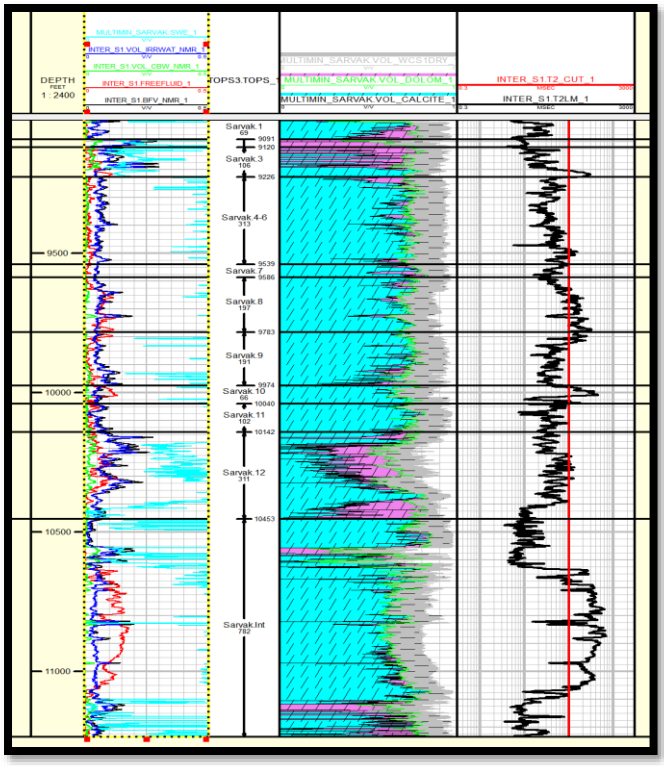

Fig. 10. Comparison of water saturation curves obtained from NMR tools and water saturation curves obtained from resistivity tools.

4.3. Identification of potential low-resistivity zones by comparing the results of conventional well logging and NMR

One advantage of magnetic resonance imaging is its capability to offer precise estimations of porous spaces, enabling a thorough evaluation of fluid saturation producibility in reservoirs. Consequently, it aids in identifying and recognizing zones with low resistivity that are still producible. As mentioned earlier, when the rock contains significant amounts of bound water, the specific formation resistivity may decrease, potentially leading to misclassification of the zone as water-bearing in initial analyses, and its exclusion from production considerations. However, MRIL data reveal the presence of water in the transition zone and the existence of producible fluids in this area.

Based on the available data shown in Fig 11, potential zones can be identified. The petrophysical evaluations conducted using conventional curves, as depicted in Fig 11, suggest an overestimation of reservoir fluid saturation, primarily indicating significant oil saturation in zones three, twelve, and the final section of the Sarvak Formation. Further comprehensive studies, such as the interpretation of magnetic resonance imaging data, can offer more accurate petrophysical parameters. A comparison of results reveals discrepancies in certain

zones between the calculated fluid saturation from NMR and the conventional curves. For instance, in zone eight of the Sarvak Formation (depth interval: 9586 to 9783 ft), the resistivity curve indicates water saturation in the reservoir, while NMR investigations suggest excellent porosity and permeability in this zone. Additionally, the calculated fluid saturation points to a higher volume of fluid associated with bound waters in this zone. The T2 distribution, surpassing a threshold, indicates the presence of free fluids. Examining the viscosity curve and the shape of the T2 distribution, characterized by tall triangles with short bases, suggests the potential presence of free hydrocarbon fluids along with a partial water fraction. For a more definitive determination of fluid type, it is necessary to utilize core analysis results.

Upon further investigation, two zones (10661-10815 ft) and (10830-11063 ft) within the Int zone of the Sarvak Formation can be assessed for water saturation based on the decreased resistivity curves observed in these intervals. NMR studies suggest that a significant portion of the assessed fluids is associated with membrane pores, making them non-producible due to their non-retrievable nature. These membrane-bound fluids act as electrical flow mediators in the formation, similar to a conductor, impacting the resistivity curve.

Additionally, considering the T2 distribution crossing the defined threshold and the calculated saturation of free fluids, it can be concluded that these zones predominantly consist of bound waters, serving as a barrier to electric flow. The effect of these zones is also evident on the resistivity curve. The T2 distribution in these zones represents a significant volume of fluids with viscosity ranging from 2 to 1000 centipoise, exhibiting tall triangles with short bases. Using these two indicators, it can be confidently concluded that the reservoir fluid type includes hydrocarbons along with a partial water fraction. However, for a definitive determination of fluid type, core analysis results should be considered.

Based on the assessment of petrophysical parameters using the multimin method, zone number three of the Sarvak Formation has been identified as a high-probability reservoir zone. Moreover, a significant portion of water saturation has been estimated in this zone. However, further comprehensive studies and the interpretation of magnetic resonance imaging data have revealed that the assessed water saturation is predominantly associated with bound fluids and lacks producibility.

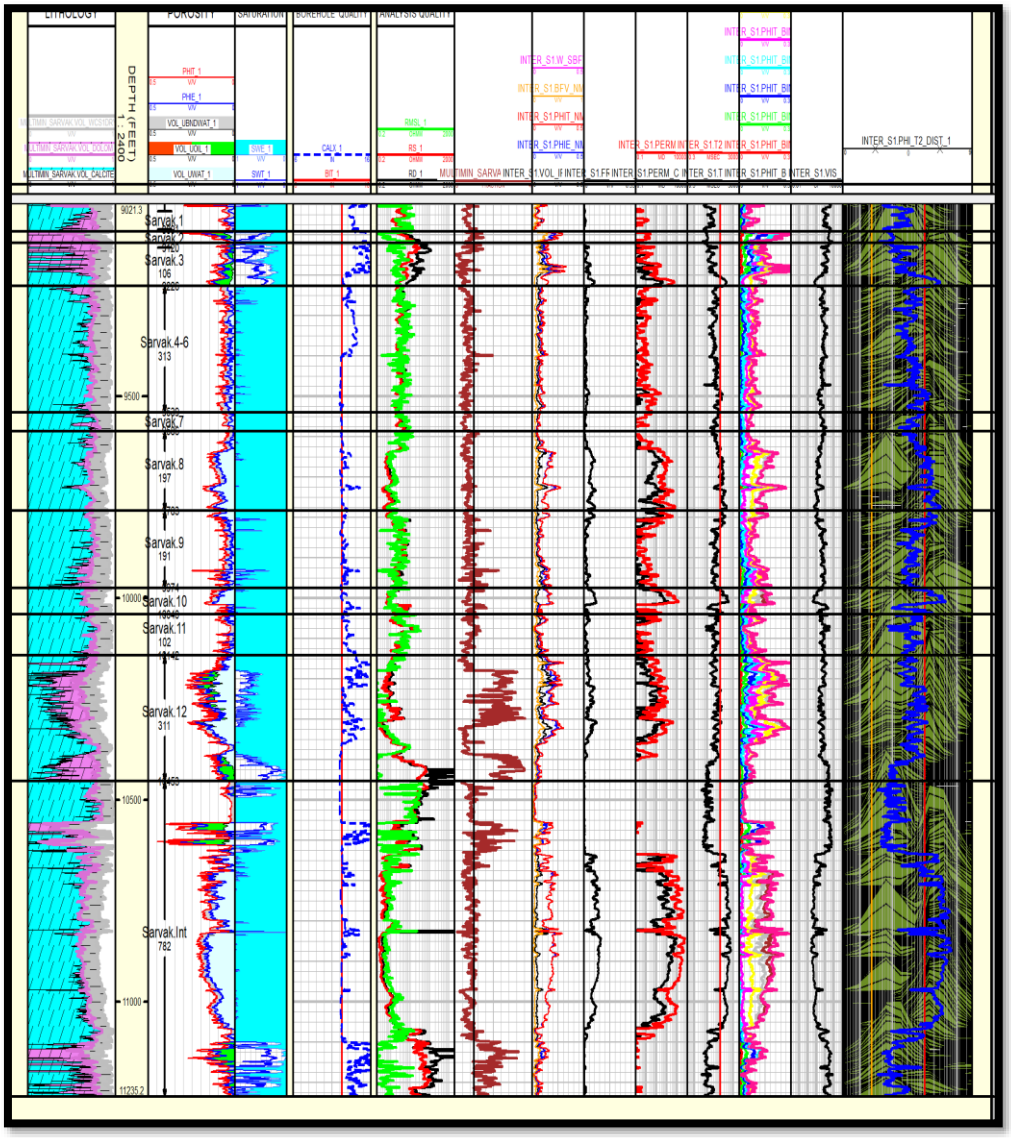

Fig. 11. Comparison of probabilistic interpretation with results obtained from the NMR log in the Sarvak reservoir of Well A.

Based on the interpretation of the NMR results alongside the results obtained from the probabilistic approach, it can be understood that in zone number four of the Sarvak Formation, considering the NMR log, which indicates low permeability, low porosity, and the absence of any producible fluid, and the fluid saturation percentage of bound fluids being close to zero, there is a discrepancy compared to the results of the probabilistic approach. The probabilistic approach recorded a higher percentage of water saturation due to the decrease in resistivity curves. The decrease in resistivity logs can be attributed to the presence of conductive minerals, as mentioned previously. In this mechanism, a high percentage of water saturation is calculated, yet the zones lack fluid producibility due to the presence of conductive minerals.

4.4. Application of Neural Networks in Estimating Petrophysical Parameters for Identifying Low-Resistivity Pay Zones

The use of neural networks is conducted in two stages. In the first stage, a small set of input and output data is employed to establish the relationship between these two categories of data, which are introduced as training samples to the neural network [26]. After training, the established relationship is applied to all input data, and the output is obtained from the neural network. It is evident that, for this purpose, a sufficient number of output samples should be available for training the network, and these samples are obtained at the location of the studied well. Therefore, in this study, the indicator values of porosity, water saturation, and permeability at well locations are introduced as training samples to the network. After training the network, the extracted relationship is applied to all seismic lines. In the analysis using neural networks, the specified indicators determined by the previous multi-attribute regression will be used. This study employs probabilistic neural networks and multi-layer feedforward networks.

Probabilistic neural networks serve as a type of data interpolation method utilized for numerical estimation in neural network approaches. Moreover, this method is suitable for estimating both continuous and discrete data. In comparison with the MLFN method, this approach offers easier and faster processing. The multi-layer feedforward neural network method closely resembles the conventional backpropagation network, and the radial basis function method is also a type of feedforward neural network, featuring a Gaussian bell curve as its primary function, akin to the probabilistic neural network. Both methods aim to enhance the spherical correlation between data indicators, differing in how the weights are calculated.

The PNN network, similar to the MLFN network, follows the data trend and exhibits less instability at the boundaries. However, its performance may decrease when the number of samples is large since it considers all training data in its domain and compares the output samples with them.

Based on the results obtained from the analysis with probabilistic neural networks and multi-layer feedforward networks in the provided Tables 4 and 5, the error percentage for each method is presented. The method with the lowest error and the highest correlation coefficient is selected for further evaluation, and by using the corresponding neural network, the results can be extrapolated to the entire seismic dataset.

Table 4. Results obtained from the analysis and estimation of the petrophysical parameter of free fluid saturation using neural network methods.

Network	Type	Final Attribute	Error	Correlation
Network_Sat	PNN	1/Inverted	0.008	95.8%
Network_Sat	MLFN	1/Inverted	0.013	88.52%

Table 5. Results obtained from the analysis and estimation of the petrophysical parameter of porosity percentage using neural network methods.

Network	Type	Final Attribute	Error	Correlation
Network_Poro	PNN	Raw Seismic	0.017	91.6%
Network_Poro	MLFN	Raw Seismic	0.02	85%

The ultimate validation outcomes for the percentage of free fluid saturation, effective porosity, and permeability were determined through the correlation coefficient and average error between the actual and estimated values during the evaluation stage, using regression and neural network methods. It was observed that the probabilistic neural network approach is more practical. The neural network method exhibited superior algorithmic performance in estimating the parameters of free fluid saturation and effective porosity. This is because geological variations are non-linear, and unlike the multi-attribute approach that assumes linear changes in the subsurface, the neural network considers non-linear variations and generates the required maps. The comparison of the two methods based on the validation results, correlation coefficient, and average error for the evaluated petrophysical parameters is presented in Table 6.

Table 6. Presents a comparison of the results obtained from two methods: probabilistic neural network and multi-regression.

No	Type	Saturation	Porosity
1	PNN Correlation	95.8%	91%
2	PNN Error	0.008	0.017
3	Multi Correlation	79%	81%
4	Multi Error	0.017	0.025

Based on the available results and the plotted cross-plots between measured and predicted values in Figs 12a, b, one can conclude that the assessment of the studied parameters using the probabilistic neural network method yields high values of correlation coefficient and average error. These findings indicate the method's high accuracy in the estimation process.

In this study, NMR log data were obtained from two wells, and both wells were assessed in the Emerge module. To validate the results, the calculated outcomes for well A and well B were compared with the predicted values. To ensure the evaluation and validation under these conditions, the software randomly excludes specific data from the calculations, using them solely for validation purposes.

In Fig 13, the actual results in the wells are depicted in red, while the predicted results for Well A are presented in black and for Well B in blue. The first and second columns display the results of free fluid saturation and effective porosity in Wells A and B, respectively. It is evident that the predicted results for free fluid saturation and effective porosity have demonstrated relatively good performance. However, some intervals exhibit slight differences between the obtained results and the available data. The blocky representation of the estimated plots is attributed to the lower resolution of the seismic data (approximately 10 meters) compared to the well logging data (on the order of a few centimeters). Overall, it can be concluded that the estimated results have provided acceptable insights into the overall trend of the variations.

The neural network method demonstrates better algorithmic performance for estimating parameters of free fluid saturation and effective porosity. This superiority arises because land changes are non-linear. In contrast to the multi-attribute method, which assumes linearity in land changes, the neural network considers these changes to be non-linear and generates the required maps [27].

The term linearity or non-linearity in the aforementioned expression is not restricted to a specific layer and does not encompass lateral changes within this layer. Characteristics of the layer, pertaining to the depositional environment and post-depositional diagenesis conditions (such as porosity as a petrophysical parameter), within a specific distance known as the radius of influence, exist in a spatial relationship—either three-dimensional or spatial. Beyond this distance, these characteristics become independent and exhibit no linear relationship between them after the impact radius.

parameters like porosity, saturation, permeability, shale volume, shear wave velocity, and length within the layer, all of which are associated with the inherent characteristics of the layer type and the depositional environment, as well as post-deposition diagenesis conditions, demonstrate a non-linear relationship in the lateral direction.

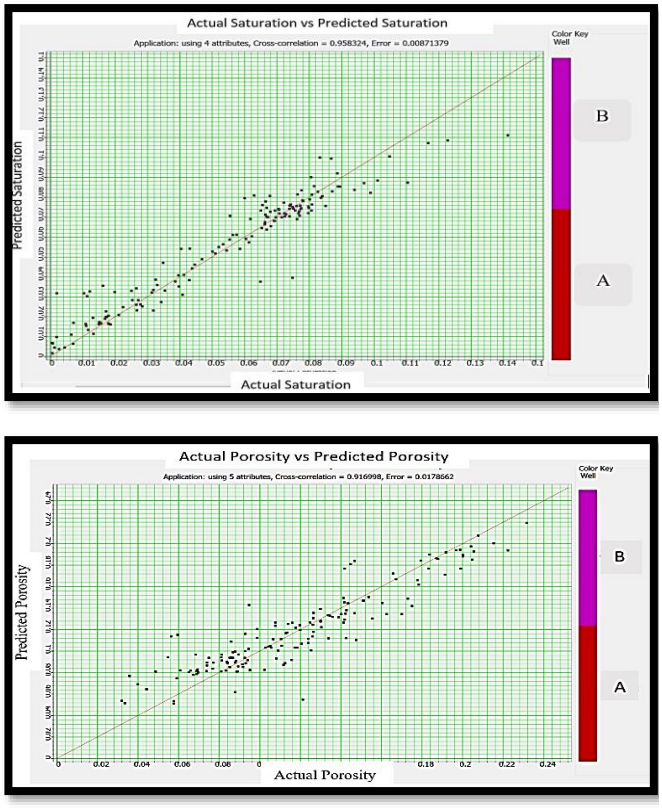

Fig. 12. a) Cross-plot of actual and predicted values of free fluid saturation using the probabilistic neural network method (Upper figure). b) Cross-plot of actual and predicted values of effective porosity using the probabilistic neural network method (Down Figure).

These lateral changes within a specific layer are of lesser significance in terms of depth. Moreover, for distinct layers that are practically situated atop one another, linear or non-linear depth changes become meaningless. This is because each layer possesses its own distinctive characteristics, and these characteristics must be assessed and compared within the layer itself under different circumstances.

4.5. Estimation of effective porosity

In Fig 14, the final results of estimating effective porosity in the Sarvak reservoir of the studied field at Well A location are displayed using the probabilistic neural network method. As observed, the porosity values cover a range from 0 to 26 percent, reflecting noticeable variability. Furthermore, upon comparing the calculated effective porosity at Well A with the estimated porosity, it can be deduced that the neural network assessment demonstrates high accuracy. Additionally, in Fig 14b, the zones from 8 to Int of the Sarvak Formation in the cross-section and Well A location are presented, revealing porosity values ranging from a minimum of 11 percent to a maximum of 24 percent.

Based on the acquired distribution maps of petrophysical parameters, specifically the free fluid saturation percentage and effective porosity percentage, derived from NMR intensity plot, the calculated porosity and permeability values in this region have been reasonably well documented. This documentation stands as a valuable reference for future studies and considerations.

4.6. Estimation of Free Fluid Saturation

In Fig 15, the estimation of the free fluid saturation percentage in the Sarvak reservoir near Well A is illustrated. The plot displays the curve of obtained free fluid saturation percentage from NMR well data in the estimated section, demonstrating that the probabilistic neural network method has delivered a reasonably accurate estimation within the

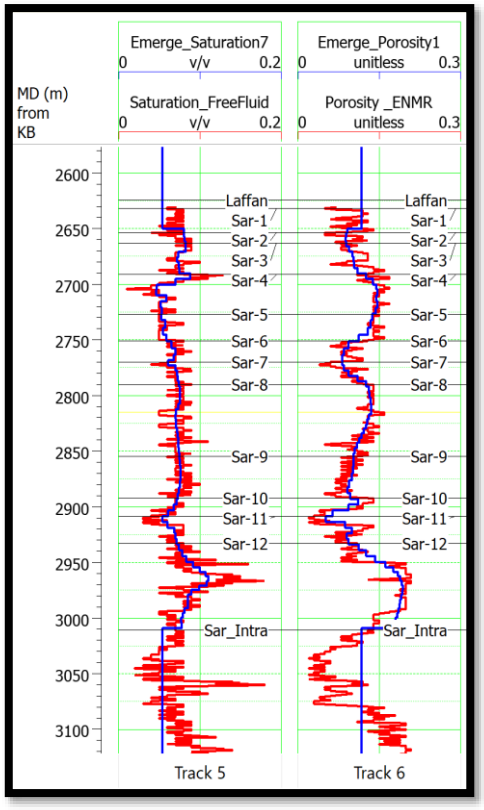

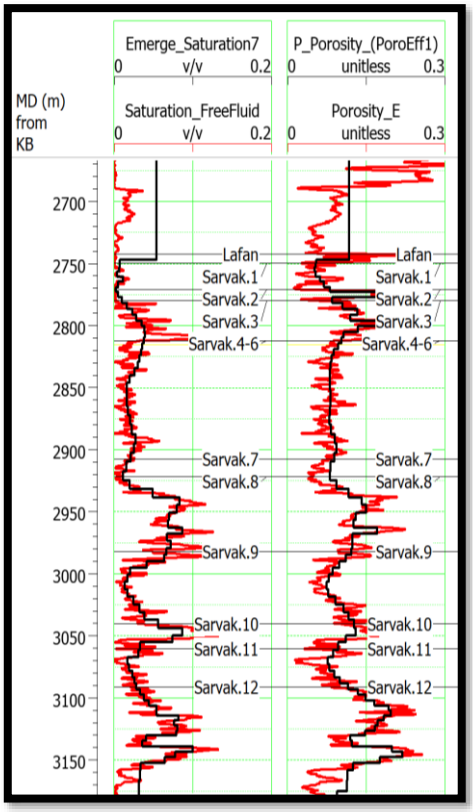

Fig 13) Comparison of predicted results with calculated values of free fluid saturation and effective porosity at Well A (Up) and Well B (Down). As evident, the predicted results for free fluid saturation and effective porosity have performed relatively well. However, in some intervals, there may be slight differences between the obtained results and the available data.

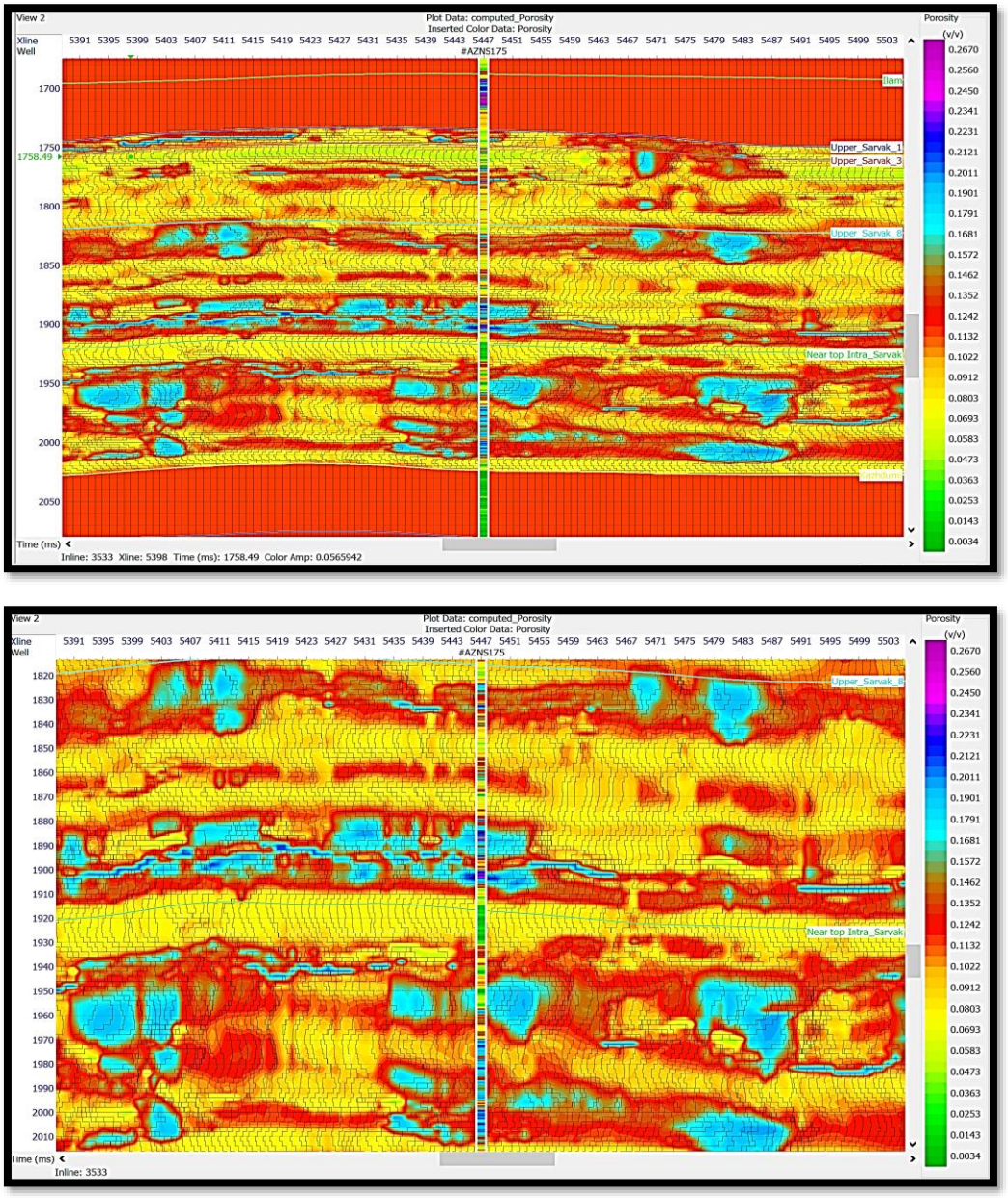

Fig. 14. a) Final results of porosity percentage prediction in the Sarvak reservoir of the studied field at the well location (Upper). b) Final results of effective porosity percentage prediction in zones 8 to Int of the Sarvak formation within the vicinity of the well A (Down).

studied area. Additionally, in Fig 15, the estimation of free fluid saturation percentage is assessed in zones 8 to INT of the Sarvak reservoir at the Well A location. According to the color guide, the color green signifies the minimum estimated value, while the color purple corresponds to the maximum estimation of 13 percent.

5. Conclusion

Based on investigations carried out in the Sarvak reservoir of the southwestern Iran field using advanced magnetic resonance imaging techniques, two potential low-resistivity zones have been identified.

Although conventional logs, including density, neutron, and resistivity logs, are highly effective in assessing hydrocarbon reservoirs, accurately determining petrophysical parameters with these logs poses challenges in low-resistivity reservoirs. To address this challenge, the utilization of Nuclear Magnetic Resonance (NMR) tools proves crucial in precisely determining fluid saturation in such low-resistivity reservoirs.

The NMR log is a valuable tool in formation evaluations, particularly for estimating and identifying low-resistivity reservoirs. Its ability to differentiate between mobile and immobile fluids aids petrophysicists in obtaining more accurate hydrocarbon reserve estimates. This is especially beneficial for identifying and estimating low-resistivity reservoirs that may present challenges with conventional logging methods. Nevertheless, interpreting NMR logs requires knowledge and experience to manually select CUT OFF values, ensuring the derivation of reliable results from measured and calculated parameters, particularly in carbonate reservoirs.

The results of NMR logs are significant in field evaluations. NMR can provide detailed information on porosity, making it a potential substitute for conventional porosity logs in porosity and fluid type identification. Furthermore, NMR results furnish quantitative details

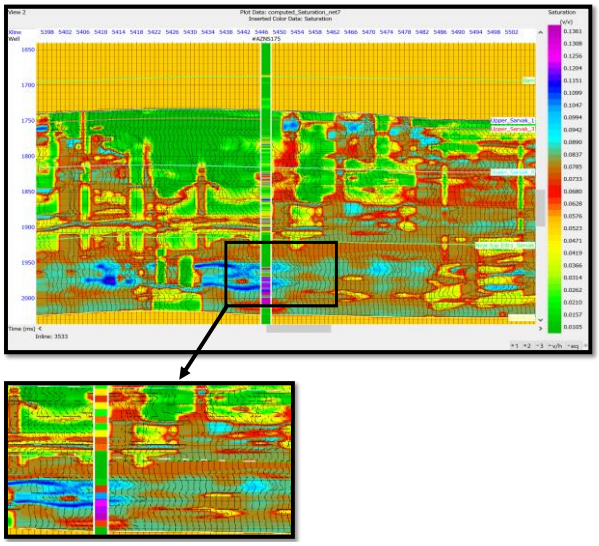

Fig. 15. Estimation of the free fluid saturation percentage in the Sarvak reservoir, the studied field within the vicinity of the well A.

about pore fluids, including clay-confined water, capillary-confined water, free water, oil, and gas. On the other hand, NMR analysis can predict the occurrence of small or water-free oil production, even in cases where the resistivity log indicates high water saturation.

Based on the obtained results in the studied Sarvak reservoir, as seen in the porosity-permeability cross plot (Fig 9), it can be concluded that the reservoir porosity is of microscopic and fracture nature, both of which are crucial factors in the formation of low-resistivity zones. Additionally, the presence of shales and clay minerals like illite and montmorillonite, which contain bound water in their micropores, is another vital factor in the formation of low-resistivity zones. The isolated micro-porosity, along with its pore water, acts as a bypass channel during fluid flow, influencing the resistivity curve and resulting in decreased apparent resistivity and calculated fluid saturation. Consequently, these zones are considered as free fluid based on the probabilistic approach and are excluded from the production cycle. However, the results of the NMR have the ability to differentiate fluids in the micro-pore spaces, which cannot be produced, from the coarse-grained porous spaces that contain free and producible fluids. This distinction indicates the amount of producible fluid in each zone. Hence, the evaluation of NMR is highly important.

In this study, due to the absence of core data, it is recommended to conduct core analysis and well testing in Well A of the Sarvak reservoir to validate and verify the results. Further laboratory studies (Routine Core Analysis, Special Core Analysis) can be performed to accurately determine petrophysical parameters such as fluid types, fluid saturation, various types of porosity, and permeability percentages. This approach will enable the precise identification and evaluation of the types of fluids present in the identified potential low-resistivity zones.

REFERENCES

[1] Robert M. Sneider, (2003), “Worldwide Examples of Low Resistivity Pay”, Houston Geological Society Bulletin, Volume 45, No. 6, Pages 47-59.

[2] Boyd et al., (1995), “The Lowdown on low-resistivity pay”, Oilfield Review

[3] Haghsenas Y., Imami N.(2019), "Reservoir Layers with Low Resistivity or Low Resistivity Contrast with Adjacent Layers: Review of Occurrence and Analysis Methods", Scientific Journal of Oil and Gas Exploration and Production. 93-86 (164).(in Persian)

[4] Khoshseima F., Kargar Z. (2013), " Calculation of Porosity and Pore Size Distribution Using Nuclear Magnetic Resonance Method, Petroleum Research, 23(73), 14 magiran.com / p1148214. (in Persian)

[5] Dehghanzadeh M., Rezaei M.(2014), "Comparison of Porosity and Permeability Obtained from NMR and Core Data in a Well in the South Pars Gas Field", Earth Science Research. 5(19), 10-15 magiran.com/p1582642. (in Persian)

[6] Razavifar M., Nikouie E., Qajari J.(2008), "Application of Nuclear Magnetic Resonance (NMR) in the Oil Industry". 158 ، ٤٧-٤١. magiran.com/p1896543. (in Persian)

[7] Zamannajad A., Mohammadi B., Kohnesal Ghadim vand N.(2007), "Petrophysical Evaluation and Comparison of Reservoir Properties Variations in Sarvak and Kazhdumi Formations in Well A of the Studied Oil Field in Southwestern Iran", Third Applied Geology Symposium. https://civilica.com/doc/34543 (in Persian)

[8] Poursiyami H., Rahimi-Bahar A.(2016),"Principles, Applications, and Processing of NMR Logs with GeoLog Software", Tehran: Petroleum Industry Research Institute. (in Persian) a book

[9] Rabani A., Eqbali F.(2007), "Geochemical Study of the Oil Field and Modeling of the Reservoir Basin", Second Iranian Petroleum Engineering Congress, Tehran. https://civilica.com/doc/146973. (in Persian)

[10] Kobraei M., Rabbani A.R, Taati.(2018), "Investigation of Production Potential in Pabdah (Turbidite) and Kazhdumi (Lower Cretaceous) Formations in the Dez Abadan Plain, Southwest Iran", Oil Research.27(93), 17-4. SID. https://sid.ir/paper/114867/. (in Persian)

[11] Sitaresmi, R., Mega, L., & Fathaddin, M. T. (2021, July). Laboratory Study: The Effect of Clay Mineral in Sandstone on Resistivity of Rock. In IOP Conference Series: Earth and Environmental Science (Vol. 819, No. 1, p. 012025). IOP Publishing.

[12] Kelishami, S. B. A., Mohebian, R., & Salmian, O. (2022). A comprehensive perspective on pore connectivity and natural fracture analysis in Oligo-Miocene heterogeneous carbonates, southern Iran. Journal of Petroleum Science and Engineering, 208, 109199.

[13] Bai Z, Maojin Tan, Yujiang Shi, Gaoren Li , Simon Clark.(2021), "Characteristics and Control Mechanism of Low Resistivity Contrast Oil Pays in Chang 8 Tight Sandstone Reservoir of Longdong West Area, Ordos Basin". Preprints 11, 2609–2620.

[14] Tan, F., Li, H., Liu, H., Jiang, F., & Yu, H. (2009). Micro-geological causes and macro-geological controlling factors of low-resistivity oil layers in the Puao Oilfield. Petroleum Science, 6, 246-253.

[15] Coates GR., Xiao L., Prammer MG.(1999), "NMR logging: Principles and Interpretation", Halliburton Energy Service, Huston, Texas.

[16] Hui, L., Rui, G., Junchang, D., Li, L. I. U., Yang, L. I. U., & Yingjie, Y. I. (2013). Productivity evaluation and influential factor analysis for Sarvak reservoir in South Azadegan oil field, Iran. Petroleum Exploration and Development, 40(5), 627-634.

[17] Abd, Muhammad Amin Nizar Bin Che, and Muhammad Amin Razak.(2012), "Evaluation of Low Resistivity Low Contrast Reservoir".

[18] Moradzadeh, Ali, Salimi Delshad, Yaser, and Kazemzadeh,

Ezzatola. (2012). Improved calculation of water saturation in carbonate hydrocarbons to well log data and laboratory assistance. Journal of Earth and Space Physics۱۲۱-۱۰۷ ،, 39(1). magiran.com/p1142031 (in Persian)

[19] Hatampour, A., Schaffie, M., & Jafari, S. (2017). Estimation of NMR total and free fluid porosity from seismic attributes using intelligent systems: A case study from an Iranian carbonate gas reservoir. Arabian Journal for Science and Engineering, 42, 315-326.٤٢ . (in Persian)

[20] Golsanami, N., Zhang, X., Yan, W., Yu, L., Dong, H., Dong, X., ... & Barzgar, E. (2021). NMR-based study of the pore types' contribution to the elastic response of the reservoir rock. Energies, 14(5), 1513."

[21] Quirein, J. A., Hampson, D., & Schuelke, J. S. (2000, August). Use of multi-attribute transforms to predict log properties from seismic data. In EAGE Conference on Exploring the Synergies between Surface and Borehole Geoscience-Petrophysics meets Geophysics (pp. cp-19). European Association of Geoscientists & Engineers.

[22] Russell, B. H. (1988). Introduction to seismic inversion methods (No. 2). SEG Books.

[23] Motiei, H. (2003). Geology of Iran, Stratigraphy of Zagros, Geological Organization of the country. A book (in Persian)

[24] Ahmad Asadi 1 Elham Asadi mehmandosti(2016). Sedimentary reservoir study of the Sarvak Formations and recognatin of its boundary with Ilam Formation by geochemical data in Chenareh anticline, south of Lorestan, 8(1), 103-135. (in Persian)

[25] Rezaei Ahmadreza (2001). Basics of Well logging In: Mohammad Lankarani editors. Petroleum geology. Alevi. Tehran University. P356. A book.

[26] Mohebian, R., Riahi, M.A., Afjeh, M. (2018). Detection of the gas-bearing zone in a carbonate reservoir using multi-class relevance vector machines (RVM): comparison of its performance with SVM and PNN. Carbonates and Evaporites 33, 347–357. https://doi.org/10.1007/s13146-017-0411-0

[27] Du, Yang, et al. "Genetic mechanism and development of the unsteady Sarvak play of the Azadegan oil field, southwest of Iran." Petroleum Science 13 (2016): 34-51. [1] Yousefi, M., Kreuzer, O.P., Nykänen, V., Hronsky, J.M.A., 2019. "Exploration information systems—a proposal for the future use of GIS in mineral exploration targeting". Geology Reviews 111, 103005.